ILLINOIS TECH | Armour College of Engineering

MMAE 414

Crop Duster

Final Report

Group 8

December 1st, 2025

Department of Mechanical, Materials, and Aerospace Engineering
Ty Garrison, Peter Mayer, Mason Rinkel, Evelina Cojocaru Visinschi, Jonah Wilkes

Contents

List of Figures

List of Tables

1 Introduction

1.1 Background

Designing a crop duster requires an aircraft that can safely and efficiently operate at low altitude while delivering agricultural products such as pesticides, fertilizers, and seeds. The design must emphasize stability, payload capability, and precise control to meet the demands of modern field application.

The previous progress achieved in the work on this project consisted of the conceptual design of a Crop Duster that meets the performance, capability, and safety requirements for an agricultural aircraft. Major sections that were part of the design such as aerodynamics, propulsion, structures, and cost analysis were discussed in the Conceptual Design Report.

In this report, the aim is to examine the system modeling for the conceptual design created earlier. First, the data was extracted from the XFLR5 design of the Crop Duster. Next, the data, such as mass properties, baseline aerodynamic coefficients, and lateral-dimensional coefficients at different angles of attack, was analyzed, and different maneuvers of the aircraft were designed. The analysis and design part listed above were realized using MATLAB and Simulink. In turn, Simulink was used to design the overall control system, as well as Thrust and Elevator, Roll, and Yaw controls.

1.2 Team Organization

Below is Table 1, which represents the team roles respected during the project work process. The roles remained the same as decided at the beginning of the project. Each section has been assigned a Lead and Secondary role.

Section	**Lead**	**Secondary**
Leader	Evelina Cojocaru Visinschi	Peter Mayer
Aerodynamics	Jonah Wilkes	Ty Garrison
Cost Analysis	Ty Garrison	Mason Rinkel
Propulsion	Mason Rinkel	Evelina Cojocaru Visinschi
Structures	Peter Mayer	Jonah Wilkes

Table 1: Team Responsibilities by Section

2 Project Summary

2.1 Project Requirements

For this project, we are focusing on two sets of requirements, divided into general and maneuver performance requirements.

General requirements for the crop duster were divided into design mission and ferry mission requirements. Design mission requirements include: operational radius of 50 nmi, design radius of 25 nmi, a minimum 15-minute fuel reserve, maximum gross weight of 19,000 lb, maximum flight speed of 250 kts, takeoff ground run $\leq$1000 ft, takeoff distance over a 50-ft obstacle $\leq$1500 ft, hard-packed dirt or grass runway surface, must dust 400 acres of land, operate under ISA conditions at 1791 ft elevation, comply with FAA 14 CFR Part 137, probability of Hull Loss less than 1×10^{-9} flight hours, Probability of Fatal Event $\leq 1 \times 10^{-6}$ flight hours. Ferry design requirements, distinct from design mission, include: cruise range 600 nmi, flight altitude ISA, 1000ft elevation, 30°F, minimum one pilot, full visibility, and safety compliance, fully reversible or fly-by-wire control system, Probability of Fatal Event $\leq 1 \times 10^{-9}$ flight hours, and accordance

to FAA 14 CFR Part 137. Each of these requirements were achieved in the previous Conceptual Design Report

The maneuver requirements put emphasis on Glide, Level Flight and Climb, Hold, and Landing. Glide should be initiated at 5,000 ft AGL. For Level Flight and Climb begins at 1500 ft AGL for 10 s, then climbs to 3500 ft. The angle of attack should never exceed 15 degrees, and the elevator deflection angles should never exceed $\pm 25°$. Hold pattern is initiated at 3500 ft AGL and approximately 165 kts, while performing 3°/s left turns, and maintaining 3500 ± 50 ft AGL. Landing is a left-hand landing pattern that starts at 2000 ft AGL and 45°, modeled in a full 6-DOF simulation with aileron, rudder, and thrust inputs, while bank angles $\leq 60°$.

2.2 Performance Parameters

As earlier progress on this project, a crop duster that meets modern performance and safety standards was designed. For this crop duster, NACA 4415 airfoil, PT6A-67F turboprop engine, and 72.2 ft wingspan were chosen, as result of the conceptual design achieved. These collectively provide a balanced combination of lift capability, stability, and propulsion performance suited to low-altitude agricultural operations. Finite element and performance analyses demonstrate that the proposed configuration achieved the required structural strength, stiffness, and maneuvering capability.

Using the aerodynamic data generated in XFLR5, the full configuration was implemented in a 6-DOF Simulink model to assess the aircraft's dynamic behavior across the required maneuver set. Within this simulation environment, the aircraft must be capable of maintaining a trimmed glide from 5,000 ft AGL, sustaining level flight at 1,500 ft AGL before initiating a commanded climb to 3,500 ft, performing a standard-rate 3°/s left turn for hold entry and outbound/inbound legs, and flying a left-hand landing pattern beginning at 2,000 ft AGL with bank angles not exceeding 60°. Across all maneuvers, the aircraft must remain within prescribed limits on angle of attack, elevator deflection, thrust capability, and altitude deviation. The performance parameters established here define the criteria against which the subsequent sections of this report evaluate the detailed glide, climb, hold, and landing simulations, ensuring that the design satisfies both regulatory requirements and operational expectations for a modern agricultural aircraft.

2.3 Payload Capabilities

Due to our payload weight being on the smaller side to maximize maneuverability and minimize takeoff distance, we looked for a pesticide for our spray system that would be both low in density and not need a ton of active ingredient weight. This would allow us to cover the 400-acre field without exceeding our 4000lb payload design.

From the pesticide data (see Appendix Figure 4), we decided to go with a pesticide that used Chlorantraniliprole as its primary active ingredient. Another reason for selecting Chlorantraniliprole is that it is one of the safer options. It works by targeting specific receptors in insects that would require a much larger dose to have any noticeable effect on mammals. The commercial brand we chose is Coragen eVo insect control [3].

To cover the entire 400-acre field, we found that we would need to use 1.1 Gallons Per Acre (GPA) of water to mix with 22.4lbs of active ingredient. This is lower than recommended if using normal nozzles, so to rectify this we found that we would need an Ultra Low Volume (ULV) nozzle. A ULV nozzle would allow us to atomize enough active ingredients while also keeping the water weight to only 3669.6lbs. This leaves plenty of weight for the nozzle apparatus and storage tank. For an ULV nozzle we went with the MicronAir AU7000 Atomizer (see Appendix Figure 18). From the handbook for the AU7000 atomizer[1] it mentions a 15cm spray width per atomizer, so with our wingspan we would be around 60 nozzles per wing and 120 overall.

3 XFLR5 Aircraft Configuration

Before building the Simulink model, the aircraft first had to be fully defined in XFLR5. The geometry in XFLR5 was created using the main design numbers from the conceptual design phase, such as the wing area, wingspan, aspect ratio, and estimated mass. The main wing uses a blended airfoil distribution, transitioning from a NACA 4415 at the root to a NACA 4412 near the tip, which gives smoother aerodynamic behavior and more realistic lift characteristics. The horizontal and vertical tails were sized using tail-sizing estimations from Raymer's Book [6], and the fuselage length was chosen to match the overall aircraft layout. Together, these inputs created a complete model suitable for stability and aerodynamic analysis.

XFLR5 was also used to determine the mass properties needed for Simulink, including the center of gravity, neutral point, and the full inertia matrix in the body frame. These values directly affect the aircraft's stability, trim, and control response, so they were taken directly from the XFLR5 mass-property calculations. After exporting and converting them into consistent units, they were used as inputs for the Simulink 6-DOF model. Table 2 summarizes the key parameters used in XFLR5 and passed into Simulink for the flight-dynamics simulations. The full XFLR5 wing profile is shown in Fig 1.

Table 2: XFLR5 configuration parameters.

Parameter	**Symbol**	**Imperial Value**	**Metric Value**
Initial mass (takeoff)	m	13000 lb	5905 kg
X-position of C.G.	X_{CoG}	2.260 ft	0.688 m
Y-position of C.G.	Y_{CoG}	0.000 ft	0.000 m
Z-position of C.G.	Z_{CoG}	0.190 ft	0.059 m
X-position of neutral point	X_{NP}	4.695 ft	1.431 m
Cruise speed	V_{cr}	165.23 kts	85 m/s
Main wing			
Wing reference area	S_{ref}	592.0 ft^2	55.00 m^2
Wing span	b	72.2 ft	22.00 m
Mean aerodynamic chord	$\bar{c}$	8.20 ft	2.50 m
Aspect ratio	AR	8.80	8.80
Horizontal tail			
Horizontal tail area	S_{HT}	150.7 ft^2	14.00 m^2
Horizontal tail span	b_{HT}	26.2 ft	8.00 m
Horizontal tail MAC	$\bar{c}_{\text{HT}}$	5.77 ft	1.76 m
Aspect ratio (HT)	AR_{HT}	4.57	4.57
Vertical tail			
Vertical tail area	S_{VT}	96.9 ft^2	9.00 m^2
Vertical tail span	b_{VT}	29.5 ft	9.00 m
Vertical tail MAC	$\bar{c}_{\text{VT}}$	6.69 ft	2.04 m
Aspect ratio (VT)	AR_{VT}	9.00	9.00
Fuselage			
Fuselage length	L_{fus}	36.0 ft	10.97 m

The inertia matrix used for the Simulink model is

$$\mathbf{I}_{\text{body}} = \begin{bmatrix} I_{xx} & I_{xy} & I_{xz} \\ I_{yx} & I_{yy} & I_{yz} \\ I_{zx} & I_{zy} & I_{zz} \end{bmatrix} = \begin{bmatrix} 27041.86 & 0 & 792.58 \\ 0 & 5528.40 & 0 \\ 792.58 & 0 & 32029.99 \end{bmatrix} \text{kg m}^2. \tag{1}$$

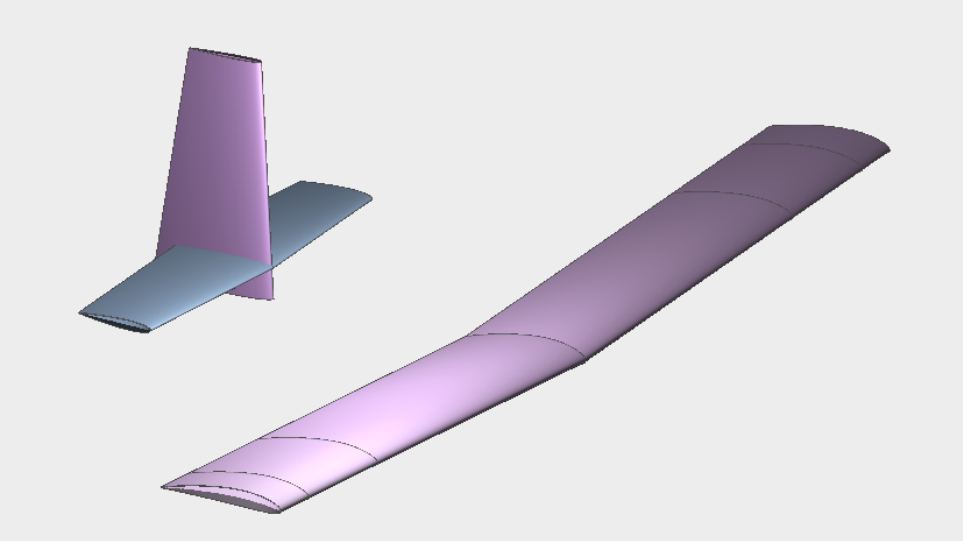

Figure 1: Aircraft profile as modeled in XFLR5

3.1 XFLR5 Data

The first set of results from XFLR5 provides the baseline (datum) aerodynamic coefficients for the aircraft with all control surfaces at zero deflection. For this configuration, XFLR5 was run over a range of angles of attack to obtain the lift, drag, and pitching–moment coefficients. The plots of $C_L(\alpha)$, $C_D(\alpha)$, and $C_m(\alpha)$ show the basic longitudinal behavior of the airplane: C_L increases approximately linearly with angle of attack, C_D follows the expected drag rise at higher lift, and C_m captures the nose–up or nose–down pitching tendency. These baseline curves are used later for trim calculations and for building the longitudinal part of the Simulink model.

A similar procedure was used to extract the lateral–directional coefficients. With all control surfaces neutral, XFLR5 was again run across angle of attack to obtain the side–force coefficient C_Y, rolling–moment coefficient C_l, and yawing–moment coefficient C_n. Although these coefficients are more sensitive to sideslip and control inputs than to α alone, the datum curves define the reference condition about which all later increments are measured. Together, these baseline C_L, C_D, C_m, C_Y, C_l, and C_n values form the core aerodynamic data set used in the simulation.

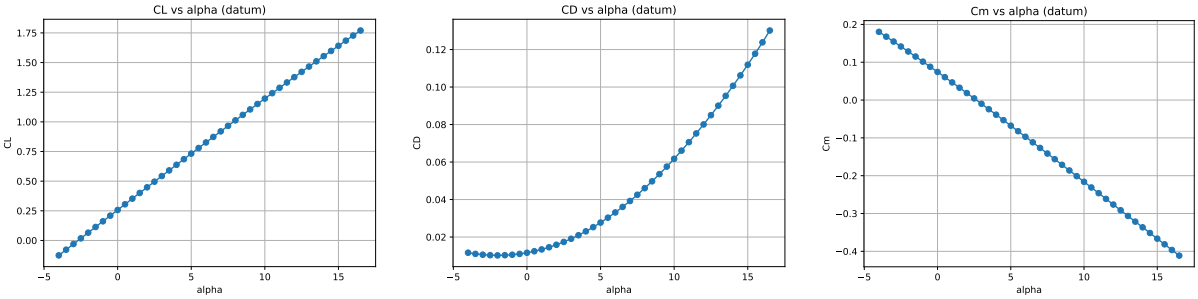

(a) C_L vs α (b) C_D vs α (c) C_m vs α

Figure 2: Baseline aerodynamic coefficients vs angle of attack

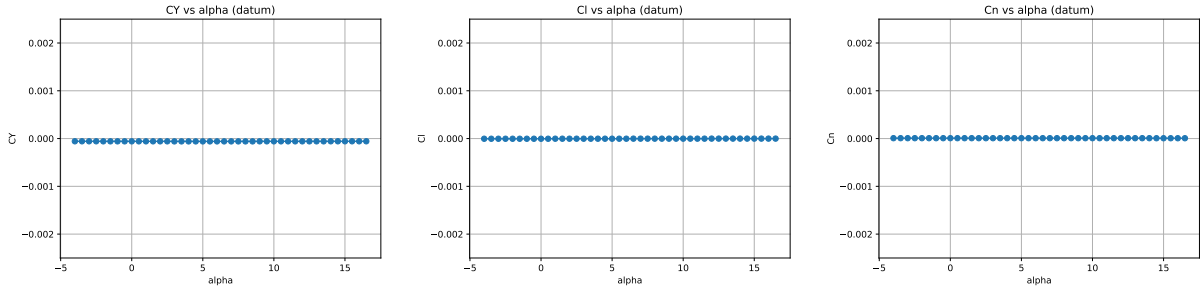

(a) C_Y vs α (b) C_l vs α (c) C_n vs α

Figure 3: Baseline lateral–directional coefficients vs angle of attack

3.2 Coefficient Increments

To use the XFLR5 data in a 6–DOF Simulink model, the baseline aerodynamic coefficients must be supplemented with increments that account for control–surface deflections and sideslip. For each case, XFLR5 was run with a single input varied—elevator, sideslip angle, aileron, or rudder—and the resulting coefficients were compared to the datum condition. In MATLAB, these increments were computed by subtracting the baseline values from each deflected case, producing matrices such as $\Delta C_L(\alpha, \delta_e)$, $\Delta C_Y(\alpha, \beta)$, $\Delta C_l(\alpha, \delta_a)$, and $\Delta C_n(\alpha, \delta_r)$. The elevator sweep ($\delta_e = -5, -3, 0, 3, 5^\circ$) produces the ΔC_L, ΔC_D, and ΔC_m variations shown in Fig. 4. These plots illustrate how the lifting, drag, and pitching-moment characteristics change with angle of attack and elevator deflection.

The lateral–directional increments were obtained in a similar manner. Figure 5 presents the effects of sideslip angles $\beta = -6, -3, 0, 3, 6^\circ$ on C_Y, C_l, and C_n, capturing the stability derivatives used for yaw and roll modeling. The aileron sweep ($\delta_a = -10, -5, 0, 5, 10^\circ$) yields the increments in C_Y, C_l, and C_n shown in Fig. 6, providing the roll-control characteristics across the angle-of-attack range. Finally, the rudder deflection sweep ($\delta_r = -10, -5, 0, 5, 10^\circ$) produces the corresponding increments in these same coefficients, shown in Fig. 7, which define the aircraft's yaw-control behavior.

Together, the increment tables in Figs. 4–7 allow Simulink to interpolate aerodynamic forces and moments for intermediate values of α, sideslip, and control-surface deflection, rather than relying on a small number of discrete XFLR5 cases. This enables a continuous aerodynamic model that accurately reflects the aircraft's response to elevator, aileron, rudder, and sideslip inputs across the full operating envelope.

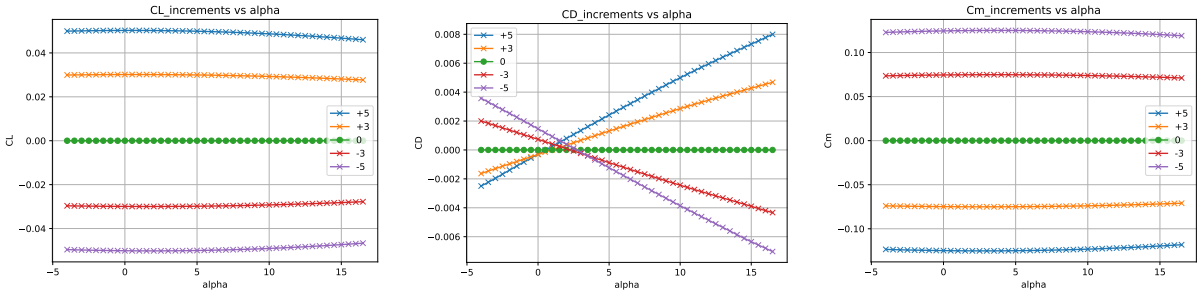

(a) ΔC_L vs α (b) ΔC_D vs α (c) ΔC_m vs α

Figure 4: Elevator coefficient increments ($\delta_e = -5, -3, 0, 3, 5°$)

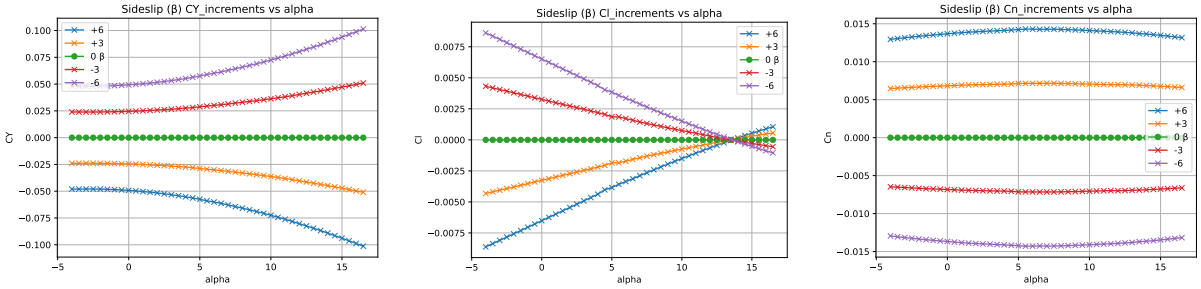

(a) ΔC_Y vs α (b) ΔC_l vs α (c) ΔC_n vs α

Figure 5: Sideslip coefficient increments ($\beta = -6, -3, 0, 3, 6°$)

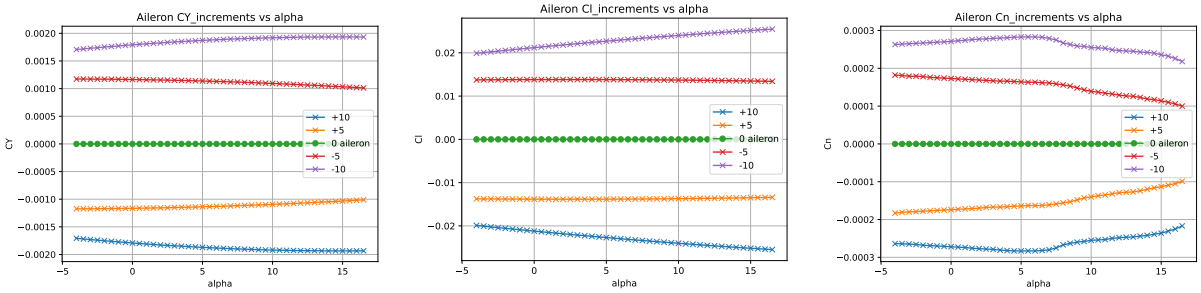

(a) ΔC_Y vs α (b) ΔC_l vs α (c) ΔC_n vs α

Figure 6: Aileron coefficient increments ($\delta_a = -10, -5, 0, 5, 10°$)

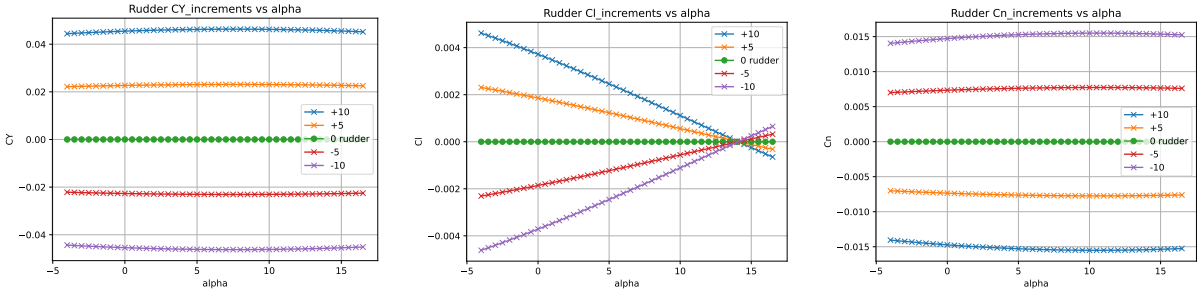

(a) ΔC_Y vs α (b) ΔC_l vs α (c) ΔC_n vs α

Figure 7: Rudder coefficient increments ($\delta_r = -10, -5, 0, 5, 10°$)

4 CAD Aircraft Modeling

The wing geometry was generated by defining airfoil cross-sections at key spanwise stations—using a NACA 4415 at the root and transitioning to a NACA 4412 toward the midspan and tip. These airfoil shapes, provided as coordinate point sets, were converted into smooth profiles and positioned along the span with proper alignment of their leading and trailing edges. The 3D wing surface was then created by lofting between these sections, producing a continuous aerodynamic transition from root to tip. Once the primary half-span geometry was formed, it was mirrored about the aircraft centerline to produce the complete wing.

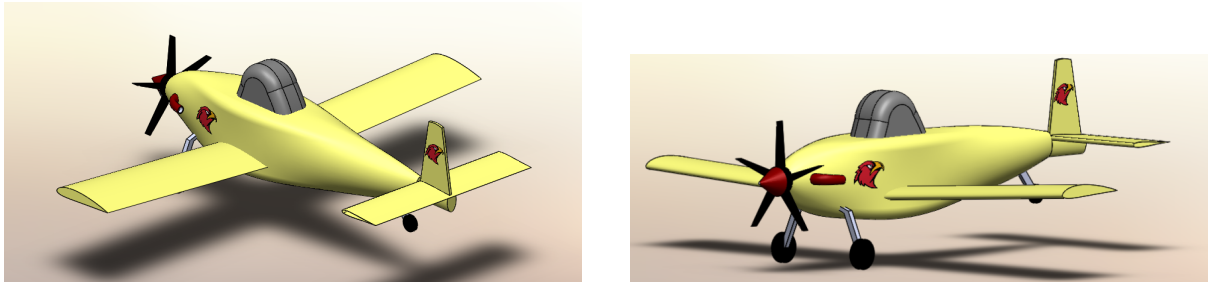

(a) (b)

Figure 8: Trimetric views of the crop duster.

Fuel-tank sizing for this aircraft is governed not by the design spraying mission but by the ferry mission, which requires the largest total fuel volume. While the design mission only consumes a fuel fraction of 0.1249, the ferry mission demands a substantially higher fraction of 0.3682 due to its 600-nmi cruise segment and extended loiter periods. Using the ferry-mission gross weight of 5,100 lb, the required fuel mass is 1,878 lb, corresponding to approximately 1.2 m^3 of avgas using a density of about 710 kilograms per cubic meter.

To house this volume within the wing while maintaining acceptable CG travel and roll stability, the fuel tanks were placed entirely within the inboard 30% of the semi-span and centered near 30% chord. This region coincides with the wing's structural carry-through and lies close to the aircraft's aerodynamic center, minimizing CG migration as fuel is consumed. A single large inboard tank alone could not meet the full volume requirement without either extending too far outboard or compromising the allowable chordwise envelope, so two additional auxiliary tanks were added. These auxiliary tanks were mirrored about a line perpendicular to the chord to keep the fuel load laterally symmetric. This prevents asymmetric roll inertia buildup and maintains good handling qualities throughout the mission. Each tank was also tapered with span to respect the reduction in airfoil thickness and avoid locating fuel mass too far outboard.

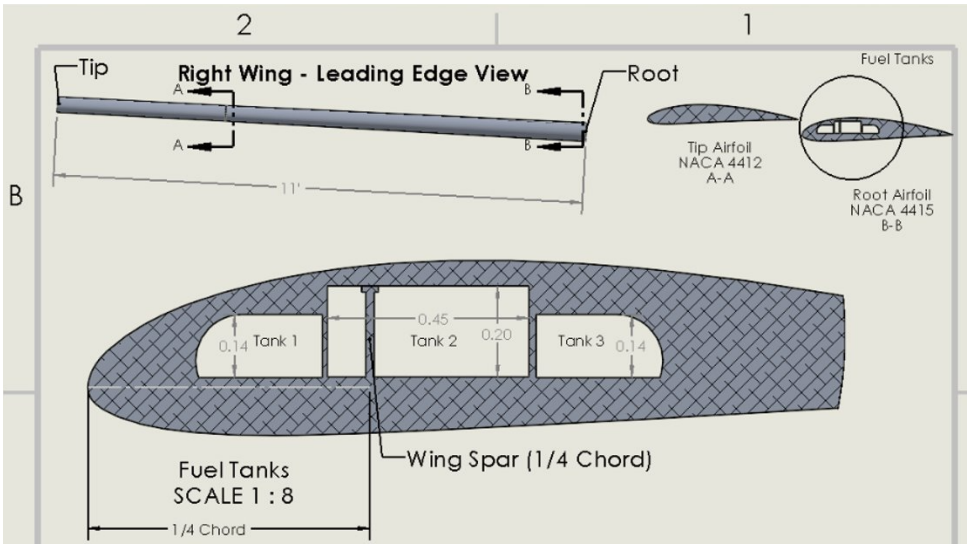

Figure 9: Drawing illustrating dimensions of fuel tanks relative to chord.

Tank sizing was finalized using a volume-subtraction method directly in SolidWorks. The total wing volume was computed, the tank geometries were cut into the wing, and the remaining wing volume was monitored. By adjusting the dimensions and taper of the three-tank system, the internal cavity volume was iteratively tuned until it matched the required ˜1.2 m^3 of fuel. The resulting three-tank configuration satisfies the ferry-mission fuel requirement while maintaining correct mass placement, good static and dynamic stability characteristics, and manufacturable geometry fully contained within the inboard wing structure. Additional geometric views, including the side-by-side airfoil sections and the trimetric fuel-tank layout, are provided in Appendix A.3 (Figures 19 and 20).

The hopper volume is dictated directly by the aircraft's payload capacity, since nearly all of the usable payload on a crop-duster is liquid chemical. Our design mission uses a 4,000-lb payload, which—assuming a typical agricultural spray density of about 8.5 lb/gal—corresponds to roughly 470 gallons of effluent. Converting this volume to cubic feet using 7.48 gal/ft^3 yields approximately 55–60 ft^3 of usable tank volume. This provides a clear, requirement-driven basis for hopper sizing that is fully tied to the weight assumptions already used in the initial sizing analysis. Tank sizing was finalized using a volume-subtraction method directly in SolidWorks. The location of the hopper was chosen to be directly behind the firewall of the engine and under the cockpit per the National Agricultural Aviation Association (NAAA).

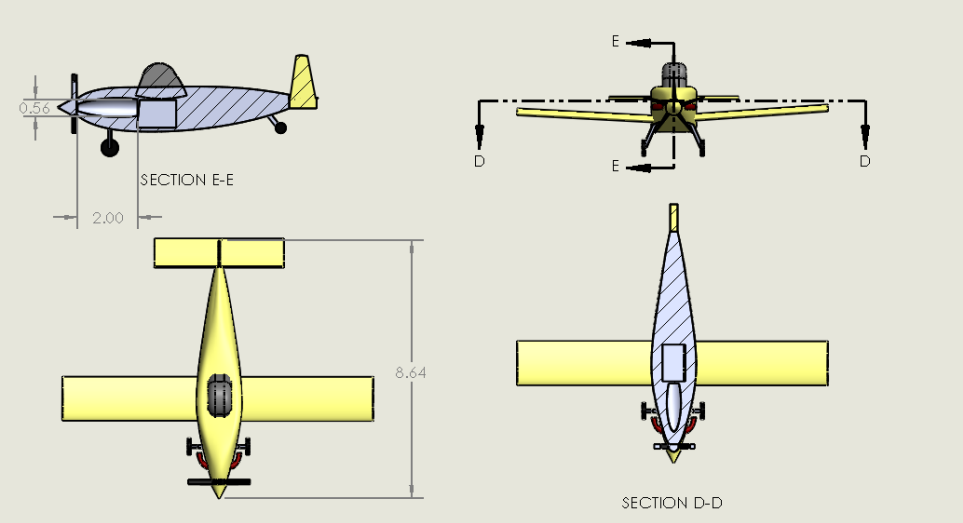

Figure 10: Drawing illustrating size and location of engine and hopper displacement.

The PT6A-67F turboprop we chose has dimensions of 1.98 m × 0.48 m × 0.56 m. To house this, we used a bullet-shaped volume measuring 2 m in length and 0.56 m in diameter to perfectly fit the engine as seen in the drawings above.

5 Aircraft Performance

5.1 Simulink Control

To model the crop duster's maneuvering performance, we implement a full 6-DOF Simulink aircraft model using the previously defined datum conditions as the initial state. The model is driven by three coordinated control subsystems—Thrust/Elevator, Roll, and Yaw—each providing closed-loop regulation of the aircraft's longitudinal and lateral–directional motion (Fig. 11).

The Thrust and Elevator Control subsystem (Fig. 12a) governs altitude and airspeed. Measured altitude and forward velocity are compared to commanded values, and PID controllers adjust thrust and elevator deflection accordingly. Because pitch attitude and thrust are coupled, these two loops work together throughout all maneuvers to hold the desired climb, glide, or landing speeds.

The Roll Control Loop (Fig. 12b) uses roll angle and roll rate feedback to generate the aileron command. For the Glide and Climb segments, the aircraft holds wings-level. During the Hold maneuver, a 24.455° bank is commanded to achieve the required 3°/s turn rate. In the Landing maneuver, a standard 30° bank is applied to realign the aircraft with the runway heading.

The Yaw Control Loop (Fig. 12c) regulates heading and yaw rate using the rudder. This loop has minimal influence in straight flight but becomes important during the Hold and Landing turns to correct sideslip and maintain coordinated flight.

These three subsystems operate together to produce stable closed-loop control for each maneuver, with block-level diagrams shown in the figures that follow.

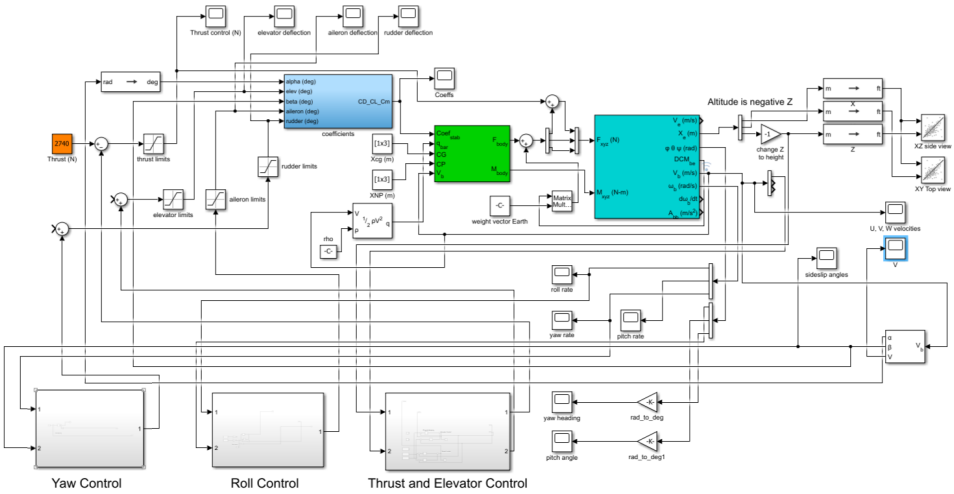

Figure 11: Overall Control System

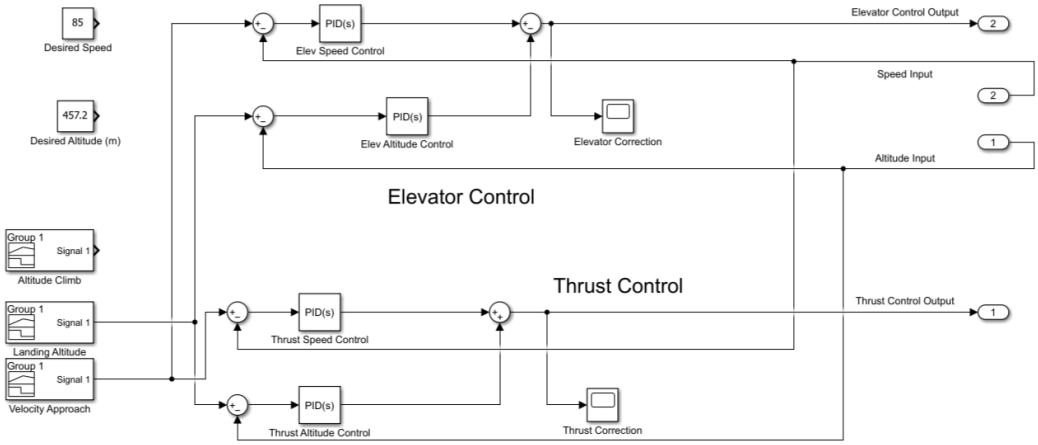

(a) Thrust & Elevator Control

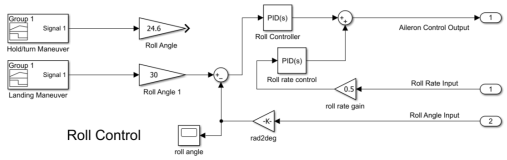

(b) Roll Control

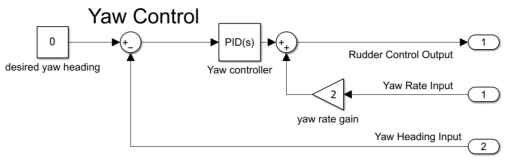

(c) Yaw Control

Figure 12: Control System Subsystems: (a) Thrust/Elevator, (b) Roll, and (c) Yaw

5.2 Glide Performance

The first step in evaluating the aircraft control architecture is to assess its natural glide characteristics. For this maneuver, only the elevator is allowed to actuate, and its role is limited to damping phugoid oscillations while the aircraft descends from an initial altitude of 5000 ft. The target glide speed is 85 m/s (≈280 ft/s), consistent with the performance requirements. As shown in Fig. 13, the aircraft quickly damps its initial transients and converges to a trimmed condition with a steady elevator deflection of +0.4525°.

To determine the glide ratio, the final 20% of the trajectory is analyzed, corresponding to the most settled portion of the motion. Over this segment the aircraft descends 961 ft while

covering 19,598 ft horizontally, yielding a slope of –0.0473. The inverse of this slope provides an L/D of approximately 21.14. Although slightly below the original conceptual design target of 25, this value remains consistent with expectations given the incremental changes made to the wing profile and aircraft mass during later design stages. All glide performance objectives were successfully met.

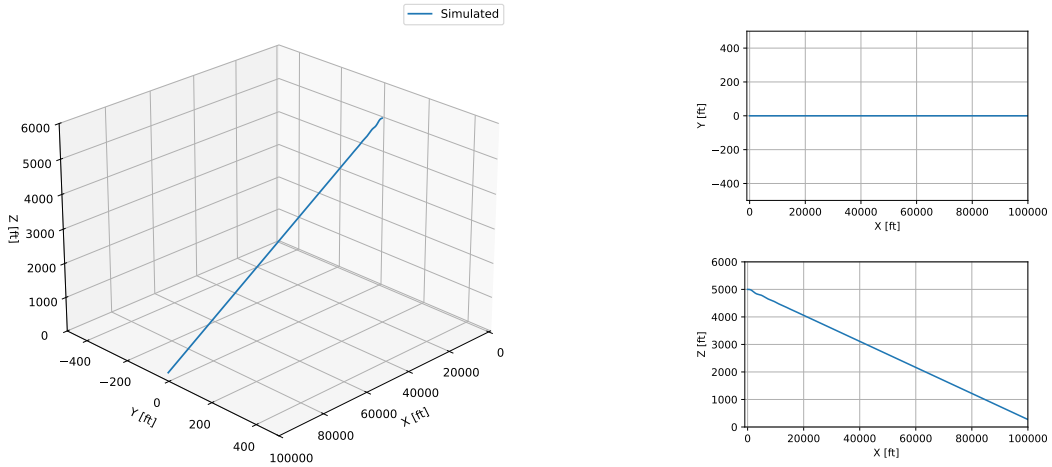

Figure 13: Glide Trajectories

5.3 Climb Performance

The next performance evaluation examines the aircraft's climb capability. Here, both elevator deflection and thrust commands are regulated through altitude and speed control loops to achieve the desired climb trajectory. Starting from 1500 ft AGL, the aircraft maintains level flight for the required 10 seconds, then transitions into a controlled ascent guided by PID-based altitude control. The aircraft reaches 3500 ft in approximately 120 seconds, corresponding to an average climb rate of 1000 ft/min.

Figure 14 shows that the simulated trajectory tracks the commanded profile with minor but expected deviations, arising from the coupled effects of elevator and throttle corrections. Throughout the maneuver, the aircraft remains within acceptable limits of angle of attack, elevator deflection, and thrust command. The climb concludes with the aircraft stabilizing at 3500 ft, fulfilling all climb performance requirements.

The detailed elevator, angle-of-attack, and thrust histories versus horizontal position are provided in Appendix A.4 (Fig. 21). During the climb, the angle of attack stays below 4°, elevator deflection remains within –7°, and thrust peaks at 8000 N—values well within the aircraft's performance limits and achieved with only minor pitch changes.

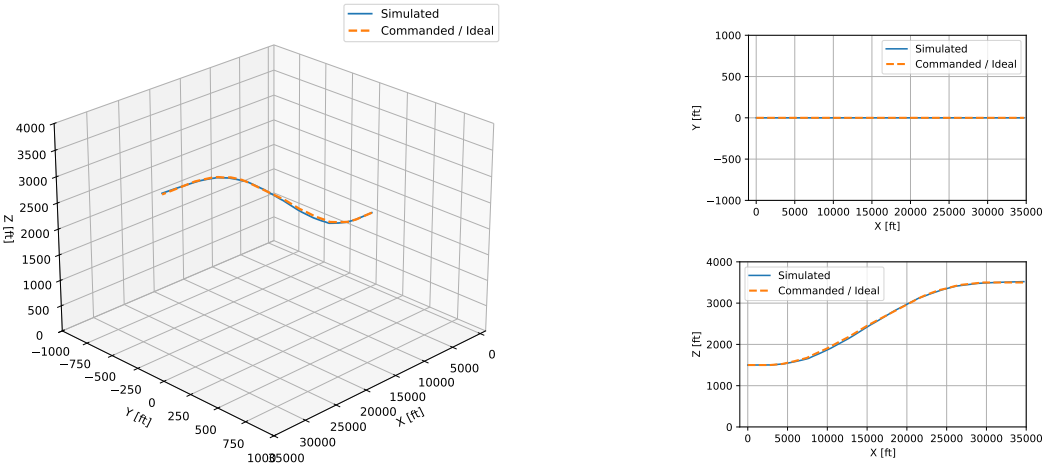

Figure 14: Climb Trajectories

5.4 Hold Performance

After verifying longitudinal performance, it is necessary to evaluate the aircraft's lateral– directional stability by introducing a controlled turning maneuver. The holding pattern is a standard aeronautical procedure used to maintain aircraft separation and delay arrivals, and for a crop duster this ability is equally important for performing repeated, level turns during field passes. This maneuver therefore serves as a practical test of the aircraft's stability and control authority in the third dimension.

Beginning from level flight at 3500 ft AGL, the aircraft initiates a coordinated 3°/s turn using a 24.455° bank angle for one minute, placing it on the reciprocal heading. It then flies straight for one minute, performs a second 3°/s turn of equal duration, and finally returns along the original track to complete the four-minute pattern. As shown in Fig. 15, the aircraft closely follows the ideal path with less than ±3 ft of altitude deviation.

Control allocation remains consistent with earlier maneuvers: elevator deflection maintains altitude, thrust regulates speed, ailerons hold the commanded bank angle (Fig. 12b), and rudder control keeps the sideslip angle near zero (Fig. 12c). The aircraft completes the pattern within approximately 10 ft of its starting point, demonstrating stable lateral–directional behavior and meeting all hold-maneuver requirements.

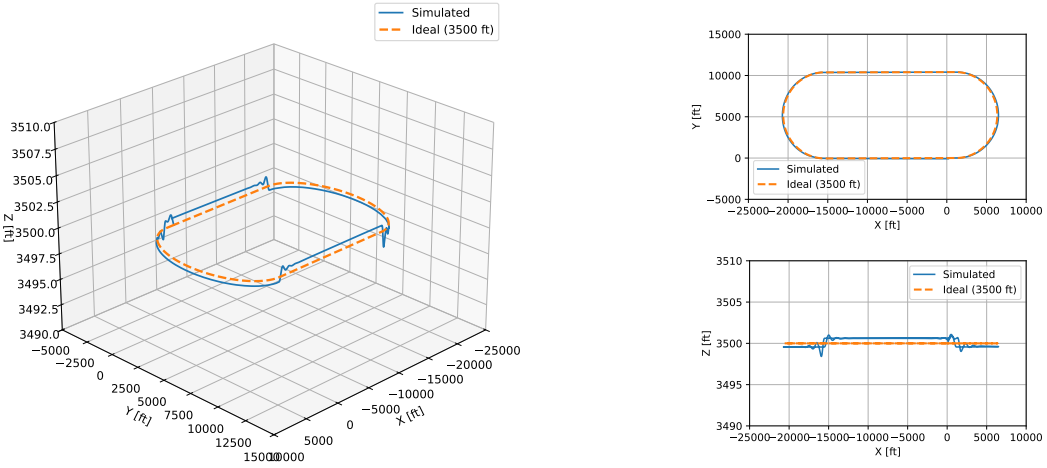

Figure 15: Hold Trajectories

5.5 Landing Performance

The final maneuver combines the lateral and longitudinal control elements in a full landing pattern. Starting at 2000 ft AGL and cruising at 85 m/s, the aircraft performs a 45° left turn over 15 seconds using a 30° bank. It then descends 1000 ft over approximately 50 seconds while flying parallel to the runway. After leveling near 1000 ft AGL, the aircraft performs two 90° turns—each using the same 30° bank—to transition onto the base and final approach legs. The final descent is a shallow approach, covering 1000 ft of altitude change over 150 seconds to simulate a controlled glide toward the runway threshold.

Figure 16 shows that the simulated trajectory closely follows the ideal pattern with minimal deviation. The maximum descent rate remains below 1000 ft/min, lower than the climb performance check and satisfying operational constraints. During the final segment, the aircraft settles to a landing speed of approximately 40 m/s (≈77 kt) with zero thrust. Although this speed is slightly higher than ideal for a crop duster, the model does not incorporate flap deployment, which would ideally reduce approach speed by at least 10 m/s (to ≈58 kts) and bring touchdown conditions into the desired range.

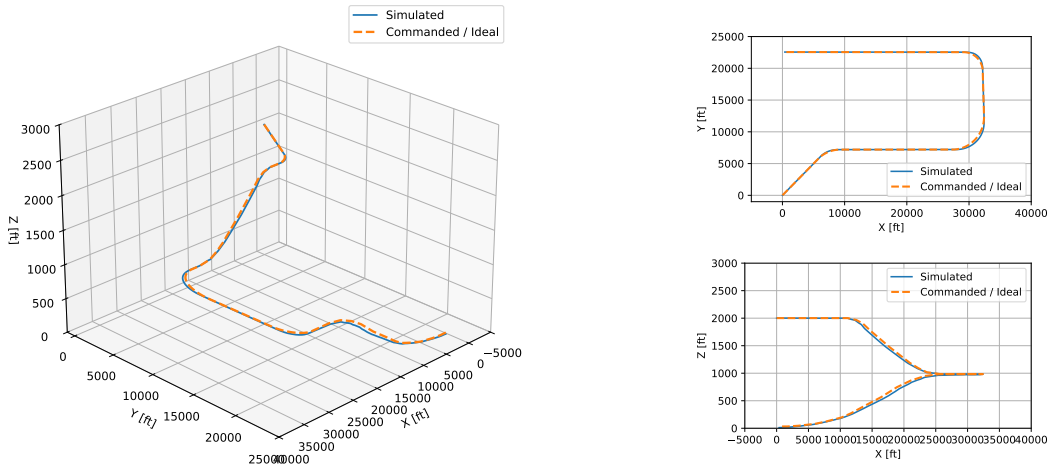

Figure 16: Landing Trajectories

Overall, the aircraft demonstrates stable and well-controlled behavior across all evaluated maneuvers, including glide, climb, hold, and landing operations. In each case, the simulated trajectory remains close to the ideal guidance path, with only minor deviations arising from expected control-system interactions. The results confirm that the control architecture provides adequate control response in both the longitudinal and lateral–directional axes, and that the aircraft meets all mission performance requirements. These findings indicate that the design is robust, operationally realistic, and ready for further refinement and eventual field testing.

6 Risk Analysis

The success of our aircraft design depends on ensuring that the plane is safe, reliable, and capable of meeting all mission profile requirements. Because crop dusters regularly operate at low altitudes, have multiple obstacles in their flight path, and large payloads the team created a risk assessment to identify, assess, and mitigate the large number of possible hazards. To develop this assessment, the team followed the Department of Defense (DoD) System Safety Standard MIL-STD-882E [4], which is the DoD's standard for system safety engineering. The Purpose of the standard is to provide a structured method for identifying hazards, classifying their risk level, and determining appropriate mitigation strategies.

Under MIL-STD-882E, each hazard is assigned both a severity level and probability level as seen by Table 5 in Appendix A.5, which shows each level and its definition. Severity measures the consequence of the hazard and how series the outcome would be if it occurred. Probability measures how likely the hazard is to occur. Once the severity and probability level are determined for a hazard it is placed into the USAF Airworthiness Risk Assessment Matrix (Table 6 in Appendix A.5) and assigned a Risk Assessment Code (RAC). A hazard's RAC determines who is responsible for accepting each risk.

Using a systematic analysis, the team evaluated our aircraft throughout its entire life cycle, considering both mission profiles as well as hazards outside operations. For each mission profile, hazards were categorized into Preflight/Ground Operations, In-Flight, and Landing. Hazards ousting of the mission profiles were grouped into Design, Manufacturing, and Lifecycle categories. For every category within each profile, the most likely to happen hazards were noted and then assessed under the MIL-STD-882E. Because our aircraft is only a model with no actual test data, the probability of each hazard was based on the overall qualitative risk control section of the MIL-STD-882E [4] and data found using a special investigation report on the safety of agricultural aircraft operations [7]. With each hazard given a RAC, the data was then organized into Table 3 where the risk associated with each hazard as well as the mitigation measures was noted. Each mitigation measure was decided by considering cost, feasibility, and effectiveness of each method to determine the best options.

Table 3: Autonomous Crop Duster Risk Assessment

	Design, Build, and Upkeep of Aircraft			
	Hazard	**Assessment**	**Risk**	**Mitigation**
Design	Structural / Load Design Errors	D1	Structural failure, loss of aircraft	FEA, safety factors, design reviews
	Aero / Stability–Control Design Errors	C2	Loss of control, unsafe handling	XFLR5 validation, flight simulation
	Airplane Unable to Meet Regulations	C4	Compliance delays and use prevention	Regulatory reviews
Manufacturing	Manufacturing Delays	A4	Delayed project timeline	Backup supply chain plan for long term delays and controlled resource allocation
	Assembly Errors	B2	Loss of control / malfunctions	Checklists and verification specialists
	Faulty Components	C2	Unexpected system failure	Approved suppliers, component inspections and tests
Lifecycle	Maintenance Errors	C3	Component failure	Training, constant plane inspections
	High Operational Cost	C4	Delays and high cost flights	Budget planning, cost reductions
	Aging Aircraft / Wear	B3	Reliability degradation	Lifecycle inspections and regular maintenance
	Ferry Mission			
	Hazard	**Assessment**	**Risk**	**Mitigation**
Pre-Flight / Ground Ops	Improper Preflight Setup	C2	Takeoff or in flight failure	Checklists, pre-flight training
	Fuel / Fluid System Leaks or Spills	C2	Fire hazard, engine failure	Leak detection system, inspections, spill procedures, PPE
In-Flight Operation	Engine Failure / Power Loss	B1	Forced landing, hull loss, environmental damage	Engine monitoring systems, redundant systems, preflight engine inspections
	Navigation Instrumentation Loss	C2	Loss of navigation capability, unsafe heading/altitude deviation	Redundant instruments, cross-checking procedures, gyro/GPS backup
	Foreign Object Collision	C1	Catastrophic collision	Obstacle mapping, GPS geofencing
	Pilot Disorientation / Unable to Perform	C1	Catastrophic collision	Altitude/flight training, autonomous backup system
Landing / Post-Flight	Landing Gear Failure	D2	Gear collapse	Scheduled maintenance, tests, and inspections
	Runway / Field Obstructions	C3	Excursion risk	Field inspection, backup fuel, backup runway
	Brake / Tire Issues	C3	Overrun risk	Brake/tire checks and inspections
	Autonomous Flight			
	Hazard	**Assessment**	**Risk**	**Mitigation**
Pre-Flight / Ground Ops	Improper Preflight Setup	B2	Takeoff failure, incorrect mission initialization, incorrect spray location	Checklists, mission file verification, pre-flight trainings
	Fuel / Fluid System Leaks or Spills	C2	Fire hazard, chemical exposure	Leak detection system, inspections, spill procedures, PPE
In-Flight Operation	Engine Failure / Power Loss	C1	Forced landing, hull loss, environmental damage	Engine monitoring systems, redundant systems, preflight engine inspection
	Lost Link	D1	Fly-away, catastrophic collision	Dual-band link, lost-link protocol
	Obstacle Collision	C2	Terrain impact, structural damage	LIDAR/vision sensors, geofencing
Landing / Post-Flight	Autonomous Landing Gear Failure	D2	Gear collapse or sensor failure	Scheduled maintenance, tests, and inspections
	Obstructed Landing Zone	C3	Excursion risk	Field/landing-site inspection, backup fuel, backup runway
	Chemical Spill During Recovery	C3	Environmental contamination	Spill procedures, PPE

7 Simple GPS Positioning Testing

In order to evaluate how a realistic GPS solution would behave along the landing trajectory, a pseudorange simulation was constructed around the recorded ENU path. The true landing positions (in feet) were converted to meters and used as the reference receiver trajectory in ECEF coordinates, and a notional 32-satellite GPS constellation was defined. At each epoch, line-of-sight vectors to all visible satellites were computed, and the ideal geometric ranges were perturbed with receiver noise, satellite and receiver clock offsets, and elevation-dependent iono-

spheric and tropospheric delays on the order of a few meters (tens of feet), consistent with typical single-frequency GPS error sources [5]. The iono–tropo models were selected to match the performance of an aviation-grade GPS receiver, with slightly conservative values included to account for unmodeled or worst-case environmental effects.

The simulated pseudoranges were first processed with a position-only weighted least-squares (WLS) solution to obtain an initial ECEF estimate and an approximate ENU covariance. These values then initialized a pseudorange-based extended Kalman filter whose state includes receiver position, velocity, clock bias, and clock drift. The EKF propagates using a constant-velocity, linearly drifting clock model and applies updates using the same pseudorange data, elevation-based weighting, and ionosphere/troposphere models used in the simulator. Final EKF positions and 1–σ ENU covariances are reported in feet for direct comparison to the landing trajectory.

The primary EKF results are shown in Fig. 17, which combines the 3D ENU trajectory and the full East/North/Up time histories. These plots show that the EKF solution remains within its predicted 1,σ bounds for most of the run and closely tracks the true landing path. Additional diagnostics—including a zoomed view of the final approach (Fig. 22) and the instantaneous 3D ENU error profile (Fig. 23)—are provided in Appendix A.6 to see filter convergence and absolute positioning accuracy.

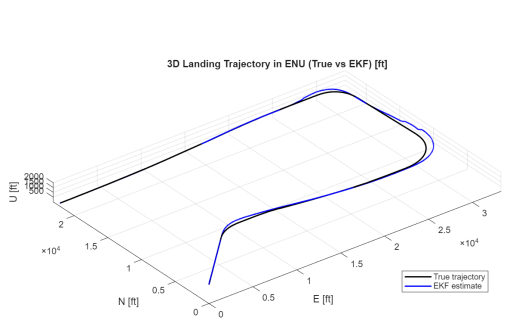

(a) Three-dimensional landing trajectory in ENU, showing the true path and the EKF position estimates.

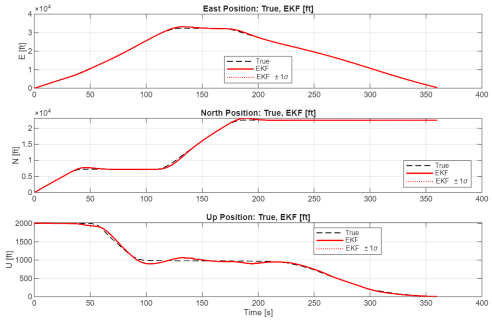

(b) East, North, and Up positions versus time for the full landing run, comparing the true trajectory to the EKF estimates and their 1 σ ENU covariance bounds.

Figure 17: EKF-based GPS position estimates along the landing trajectory.

8 Conclusions

In this report, we advanced the Group 8 crop duster from a conceptual design to a fully modeled and simulated aircraft and confirmed that it meets the stated mission, performance, and safety requirements. Using XFLR5, we defined the final geometry, airfoil distribution, mass properties, and aerodynamic coefficients for the NACA 4415/4412 wing, PT6A-67F engine, and 72.2 ft span, then carried these directly into a 6-DOF Simulink model with continuous aerodynamic coefficient and control-surface increment tables. Parallel CAD work sized and located the hopper and a three-tank inboard fuel system to satisfy the 4,000 lb payload, 400-acre coverage, and 600 nmi ferry range requirements while maintaining acceptable CG travel and stability.

Within this framework, we implemented coordinated thrust/elevator, roll, and yaw control loops and evaluated the full required maneuver set. The glide from 5,000 ft AGL trimmed near 85 m/s with a steady elevator of $\approx 0.45°$ and produced an effective $L/D \approx 21.1$, satisfying glide objectives. The climb maneuver carried the aircraft from 1,500 ft to 3,500 ft in about 120 s (≈1,000 ft/min) while keeping angle of attack below 4°, elevator deflection within about $-7°$, and thrust under 8,000 N. The 3°/s holding pattern at 3,500 ft AGL maintained altitude within roughly ±3 ft and returned to the start point within about 10 ft, demonstrating stable

lateral–directional behavior. The landing pattern met the bank-angle and descent-rate limits and achieved a final approach speed of ~ 40 m/s, with the remaining shortfall relative to ideal crop-duster speeds attributable to the absence of modeled high-lift devices and therefore a clear target for future refinement.

Finally, a risk assessment based on MIL-STD-882E and the USAF Airworthiness Risk Assessment Matrix identified key hazards across operations and lifecycle and paired them with appropriate mitigations consistent with FAA 14 CFR Part 137 and the specified probability-of-loss targets. Overall, the combined aerodynamic modeling, control-system design, maneuver simulations, payload and fuel integration, and risk analysis demonstrate that the proposed crop duster is a stable, well-controlled, and operationally capable aircraft that satisfies performance and safety requirements and forms a solid baseline for further development.

References

[1] Micron Sprayers Limited. (2020). *AU7000 Atomiser: Operator's Handbook and Parts Catalogue* (Issue 13). Micron Sprayers Limited, Bromyard Industrial Estate, Bromyard, Herefordshire, HR7 4HS, United Kingdom.

[2] Civil Aviation Safety Authority. (2017). *Risk Management: AWB-150A – Risk Assessment and Acceptance*. Airworthiness Bulletin AWB-150A.

[3] FMC Corporation. (2023). *Coragen® eVo Insect Control: Product Label*. EPA Reg. No. 279-9661. FMC Corporation, 2929 Walnut Street, Philadelphia, PA 19104.

[4] Department of Defense. (2012). *MIL-STD-882E: System Safety*. Department of Defense Standard Practice.

[5] Misra, P., & Enge, P. (2012). *Global Positioning System: Signals, Measurements, and Performance* (2nd ed.). Ganga-Jamuna Press.

[6] Raymer, D. P. (2018). *Aircraft Design: A Conceptual Approach* (6th ed.). American Institute of Aeronautics and Astronautics.

[7] Civil Aviation Safety Authority / Australian Transport Safety Bureau. (2014). *SIR 14/01 – Weather-Related Accidents*. Special Investigation Report SIR 14/01.

A Supplementary Figures and Tables

A.1 Pesticide Reference Table

Pesticide	Type	App Rate (lbs ai/acre)	Product Conc.	Product Density	ai Needed (lbs)
Glyphosate	Herbicide	1.20	5.4 lb ai/gal	9.0 lb/gal	480.0
2,4-D Amine	Herbicide	0.75	4.0 lb ai/gal	10.2 lb/gal	300.0
Lambda-Cyhalothrin	Insecticide	0.018	1.0 lb ai/gal	7.8 lb/gal	7.2
Chlorpyrifos	Insecticide	0.75	4.0 lb ai/gal	12.1 lb/gal	300.0
Propiconazole	Fungicide	0.094	4.0 lb ai/gal	9.2 lb/gal	37.6
Chlorantraniliprole	Insecticide	0.056	1.67 lb ai/gal	9.5 lb/gal	22.4

Table 4: Reference pesticide properties.

A.2 Nozzle and Atomizer Reference

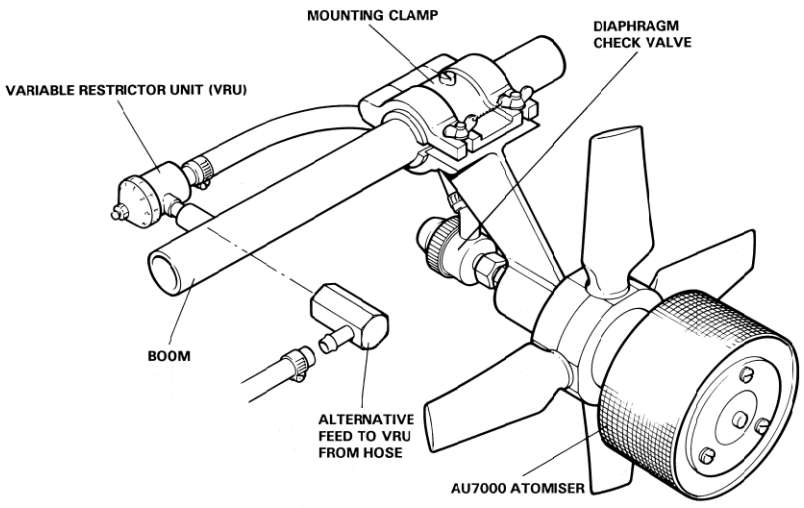

Figure 18: MicronAir AU7000 Atomizer Reference. [1]

A.3 Additional CAD Views

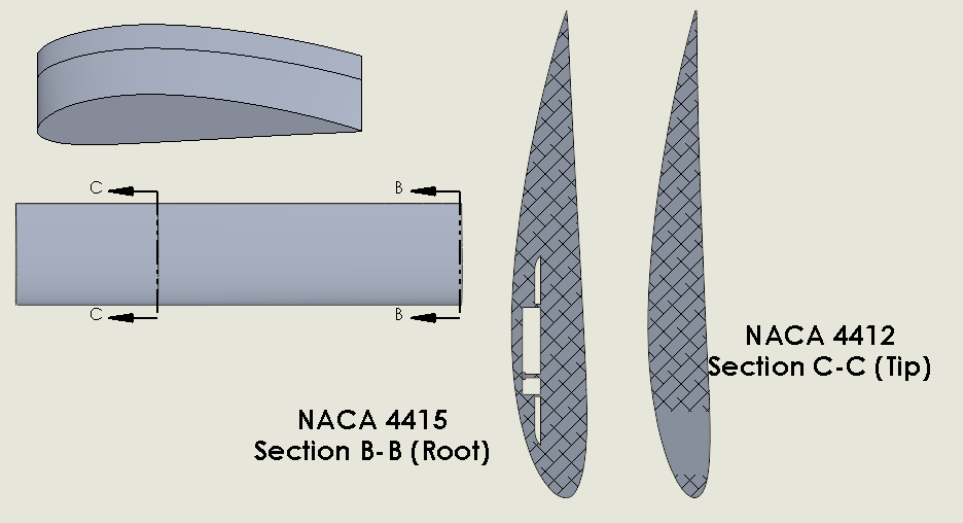

Figure 19: Side by side view of wing airfoils.

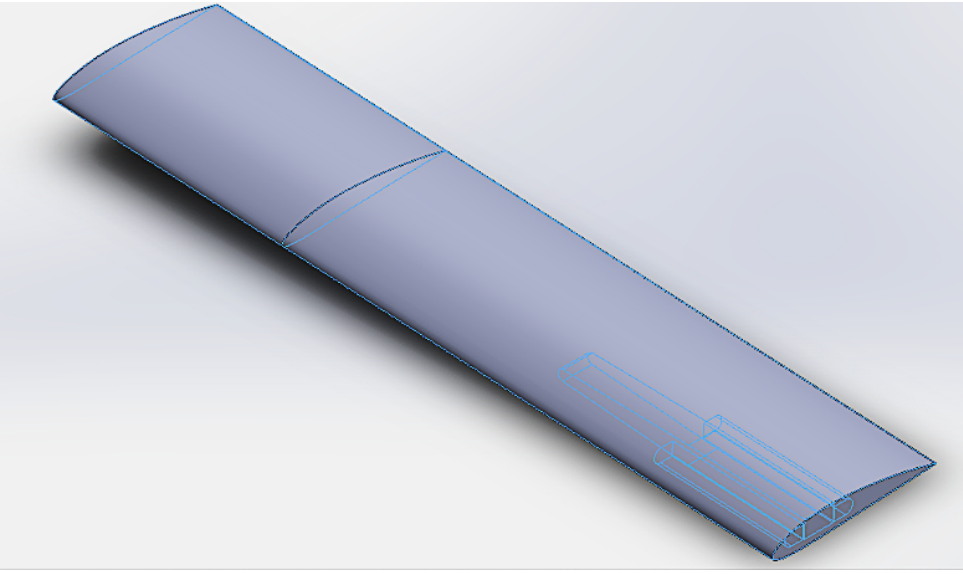

Figure 20: Trimetric view of wing showing location of fuel tanks in blue.

A.4 Control and Aerodynamic Histories

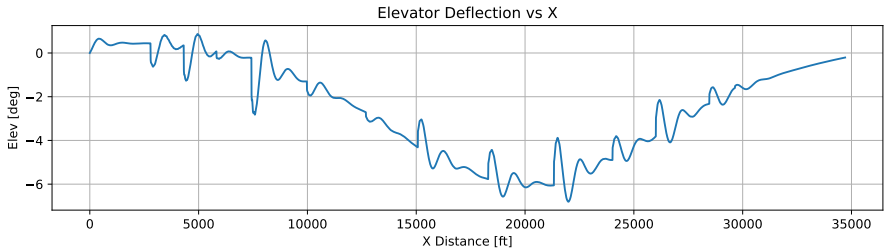

(a) Elevator vs X

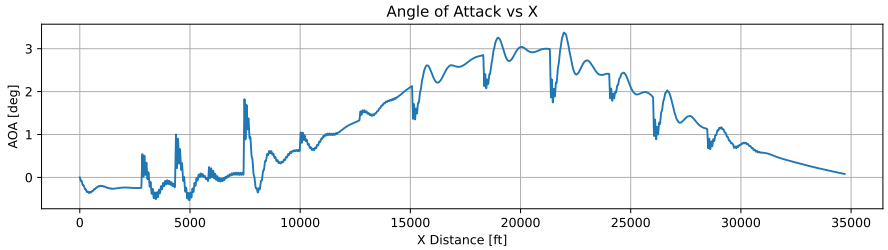

(b) AOA vs X

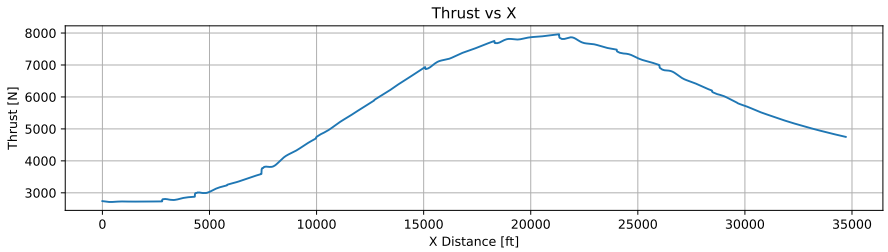

(c) Thrust vs X

Figure 21: Control and aerodynamic parameters plotted against X-position.

A.5 Risk Matrices

Table 5: Probability and Severity Definitions

Probability Definitions	
Frequent (A):	Likely to occur often in the life of an item
Probable (B):	Will occur several times in the life of an item
Occasional (C):	Likely to occur sometime in the life of an item
Remote (D):	Unlikely, but possible to occur sometime in the life of an item
Improbable (E):	So unlikely, it can be assumed occurrence many not be experienced in the life of an item
Eliminated (F):	Incapable of occurrence within the life of an item
Severity Definitions	
Catastrophic (1):	Could result in death, permanent total disability, irreversible significant environmental impact, or monetary loss equal to or exceeding $10M.
Critical (2):	Could result in permanent partial disability, hospitalization of at least three personnel, reversible significant environmental impact, or monetary loss between $1M and $10M.
Marginal (3):	Could result in injury or occupational illness causing at least one lost workday, moderate
Negligible (4):	Could result in injury or occupational illness not causing a lost workday, minimal environmental impact, or monetary loss under $100K.

Table 6: USAF Airworthiness Risk Assessment Matrix [2]

USAF Airworthiness Risk Assessment Matrix			Severity Category			
Probability Level	Probability per FH or Sortie	Freq per 100K FH or 100K Sorties	Catastrophic (1)	Critical (2)	Marginal (3)	Negligible (4)
Frequent (A)	$10^{-3} \leq$ Prob	100 ≤ Freq	1	3	7	13
Probable (B)	$10^{-4} \leq$ Prob < 10^{-3}	10 ≤ Freq < 100	2	5	9	16
Occasional (C)	$10^{-5} \leq$ Prob < 10^{-4}	1 ≤ Freq < 10	4	6	11	18
Remote (D)	$10^{-6} \leq$ Prob < 10^{-5}	0.1 ≤ Freq < 1	8	10	14	19
Improbable (E)	0 < Prob < 10^{-6}	0 < Freq < 0.1	12	15	17	20
Eliminated (F)	Prob = 0	Freq = 0	Eliminated			

High	CAE Risk Acceptance RAC = 1 - 5	Medium	PM Risk Acceptance RAC = 10 - 17
Serious	PEO Risk Acceptance RAC = 6 - 9	Low	Risk Acceptance as Directed RAC = 18 - 20

A.6 GPS Positioning Figures

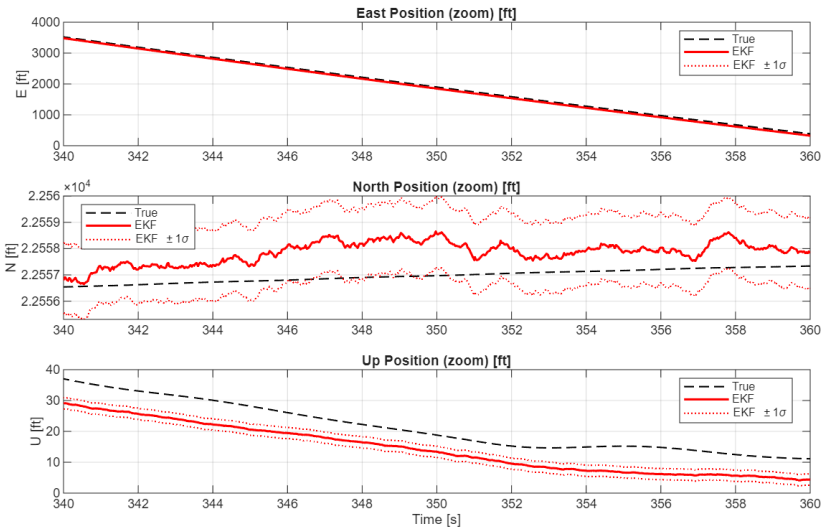

Figure 22: Zoomed East, North, and Up position histories near the end of the landing maneuver, emphasizing EKF convergence during the final approach.

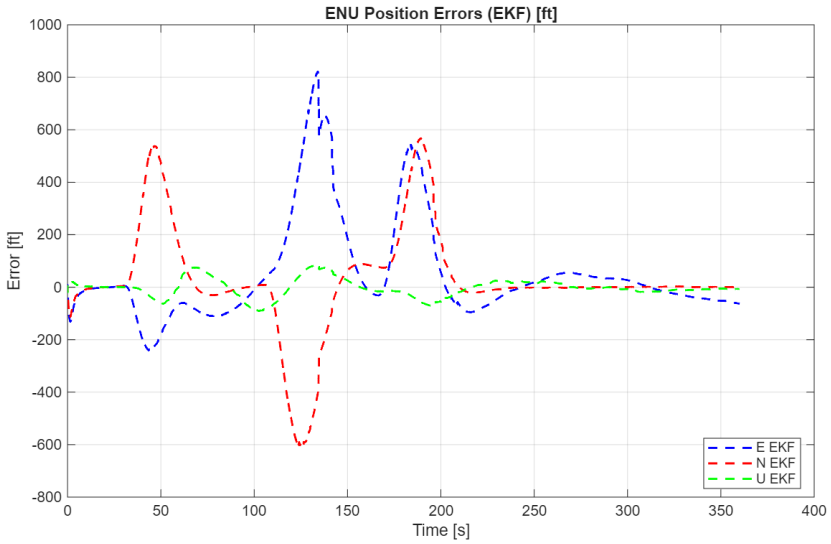

Figure 23: Instantaneous 3D ENU position error between the EKF solution and the true landing trajectory.